PERGAMON

Journal of Structural Geology 21 (1999) 351–369

JOURNAL OF STRUCTURAL GEOLOGY

Thermochronometry and microstructures of quartz—a comparison with experimental flow laws and predictions on the temperature of the brittle–plastic transition

Bernhard Stöckhert [a, *], Manfred R. Brix [a], Reiner Kleinschrodt [b], Anthony J. Hurford [c], Richard Wirth [d]

[a] *Institut für Geologie, Ruhr-Universität, D-44780 Bochum, Germany*
[b] *Institut für Mineralogie und Geochemie, Universität zu Köln, D-50923 Köln, Germany, E-mail: kleinsch@min.uni-koeln.de*
[c] *Fission Track Research Group, University College, London WC1E 6BT, UK, E-mail: t.hurford@ucl.ac.uk*
[d] *Geoforschungszentrum Potsdam, D-14473 Potsdam, Germany, E-mail: wirth@gfz-potsdam.de*

Received 11 July 1997; accepted 2 November 1998

Abstract

A gradient in quartz microfabrics across a major strike-slip shear zone (with a minor vertical component), active during the Oligocene in the Eastern Alps (Alto Adige, Italy), is correlated with new zircon fission track thermochronometric data and available Rb–Sr biotite ages to constrain the depth/temperature range of the recorded rheologic regimes. Distributed deformation in the semibrittle regime (i.e. beneath the brittle–ductile transition) is effective near the closure temperature for fission tracks in zircon (which we estimate as $280 \pm 30°C$), with high-stress dislocation creep of quartz, microcracking, and pressure solution being active simultaneously. Steady state dislocation creep of quartz at moderate stress in the fully plastic regime is effective at temperatures above the closure temperature for the Rb–Sr and K–Ar systems of biotite (ca. $310 \pm 30°C$) and below that for the K–Ar system of white mica (ca. $350 \pm 50°C$). For the inferred temperatures and correlated flow stresses derived by paleopiezometry, the majority of available experimental flow laws for wet quartzite predict strain rates on the order of 10^{-13}–$10^{-14}\,s^{-1}$, consistent with the geological constraints. This finding supports the validity of the extrapolation of experimental flow laws to natural strain rates. © 1999 Elsevier Science Ltd. All rights reserved.

1. Introduction

Predictions on the mechanical behavior of the lithosphere are based on the extrapolation of data gained in the laboratory. Such models assume that the strength of the upper crust is controlled by frictional sliding on pre-existing fractures, and that of the deeper crust by dislocation creep of an appropriate mineral aggregate (Goetze and Evans, 1979; Brace and Kohlstedt, 1980). A transitional zone of semibrittle behavior is located between the regimes of frictional sliding and of crystal plastic flow (e.g. Evans and Kohlstedt, 1995). For plastic flow of the continental crust—as a first approximation—a flow law for dislocation creep of quartz is applied generally (e.g. Meissner and Strehlau, 1982; Ranalli and Murphy, 1987).

Laboratory tests of dislocation creep in rock-forming minerals have to be conducted at high strain rates (e.g. Tullis and Tullis, 1986) and accordingly high temperatures to achieve relevant magnitudes of flow stress. Extrapolation to natural strain rates (Pfiffner and Ramsay, 1982) is over 6–9 orders of magnitude (see Paterson, 1987, for discussion). Comparison between the microstructures generated in the laboratory tests and those found in natural rocks is essential to verify identical deformation regimes (e.g. Schmid, 1982). Only when this is consistent should an established flow law be used for the extrapolation of experimental results to natural strain rates.

For quartz, the validity of the extrapolation of experimentally derived flow laws for dislocation creep can be tested by the following approaches, based on:

* Corresponding author. E-mail: bernhard.stoeckhert@ruhr-uni-bochum.de

0191-8141/99 $ - see front matter © 1999 Elsevier Science Ltd. All rights reserved.
PII: S0191-8141(98)00114-X

1. depth distribution of intraplate continental earthquakes (Sibson, 1977; Meissner and Strehlau, 1982; Chen and Molnar, 1983; Scholz, 1990);
2. correlation between quartz microstructures and thermobarometry in metamorphic rocks (e.g. Voll, 1976; Dunlap et al., 1997; G. Hirth, personal communication; this study); and
3. correlation between microstructures and in-situ stress measurements in deep boreholes (Dresen et al., 1997).

In this paper the variation of quartz microfabrics across two major slightly oblique strike-slip shear zones in the Eastern Alps is described. The minor vertical component of displacement across these shear zones has juxtaposed initially slightly different levels of the crust. The microstructural record is enhanced due to the high strain related to the strike-slip component of displacement. Simultaneous activity of both shear zones, and of related bulk deformation of the blocks in the space between, is indicated by structural and microstructural continuity and consistent with regional tectonic concepts (Ratschbacher et al., 1991).

The inferred deformation regimes along a 4 km transect range from: (1) localized brittle failure, over (2) distributed semibrittle flow with high-stress dislocation creep of quartz to (3) steady state dislocation creep of quartz at moderate flow stress in the fully plastic regime. The synkinematic temperatures are derived from new fission track data on zircon and published mica ages (Borsi et al., 1973, 1978a). Paleopiezometry and estimates on strain rate allow comparison of the results to available experimental flow laws for dislocation creep of wet quartzite and to predictions on the brittle–ductile transition (BDT) and the brittle–plastic transition (BPT) in the continental crust.

2. Geological setting

The Eastern Alps are the result of a collision between a southern continent generally referred to as Apulia (a promontory of the African plate) and the European passive continental margin after southwards

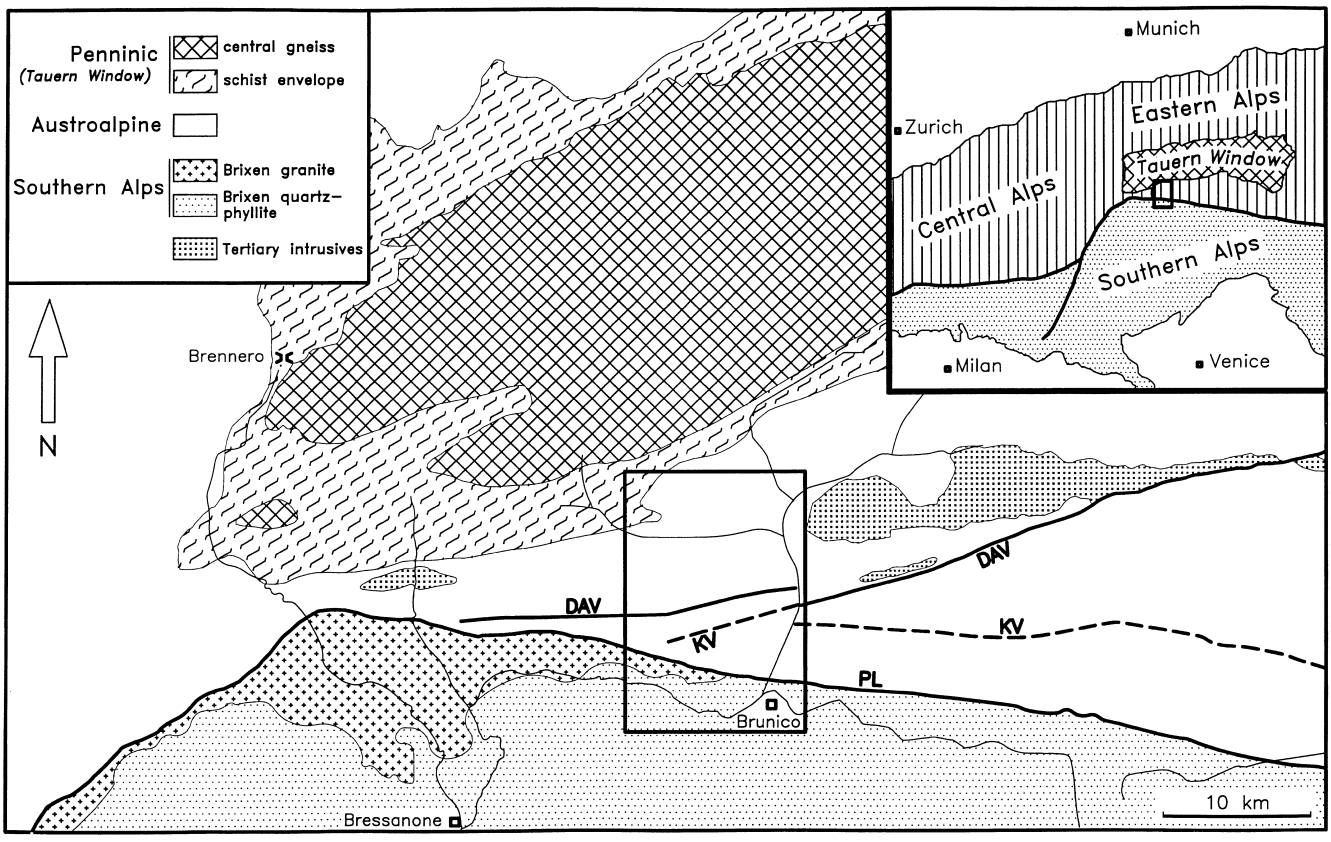

Fig. 1. Tectonic sketch map of the southwestern corner of the Tauern Window, Eastern Alps, after Bigi et al. (1973). The major faults and shear zones (PL = Periadriatic lineament, also referred to as Pustertal Line, KV = Kalkstein Vallarga Line, DAV = Defereggen Antholz Vals Line) are depicted slightly modified after Borsi et al. (1973, 1978a), Sassi et al. (1974), Hofmann et al. (1983) and Schulz (1994). The box marks the position of the studied area, that is shown enlarged in Fig. 2.

subduction of an intervening ocean (e.g. Dietrich, 1976; Frisch, 1976, 1979; Coward and Dietrich, 1989). A regional pattern of strike-slip faults developed during and after collision has been interpreted to reflect the lateral escape of continental crust towards the east (Ratschbacher et al., 1991), driven by indentation by a rigid obtuse wedge of the southern continent.

The most prominent of these fault zones, the Periadriatic Lineament or Pustertal Line (PL), separates the Eastern Alps from the Southern Alps by definition (Fig. 1). Two further major shear zones have been identified within the Austroalpine basement between the PL and the southern border of the Tauern Window (Bianchi, 1934; Dal Piaz, 1934): the Kalkstein–Vallarga Line (KV) and the Defereggen–Antholz–Vals Line (DAV). These separate the Austroalpine basement between the PL and the Tauern Window into three distinct blocks (Fig. 1), referred to as southern block, intermediate block and northern block by Borsi et al. (1973) and Sassi et al. (1974). Kleinschrodt (1987) and Ratschbacher et al. (1991) report a sinistral strike-slip character—in contrast to the dextral character of the PL—and simultaneous activity in the Oligocene/Miocene for both the KV and the DAV, between about 35 and 25 Ma.

The marked contrast in Alpine thermal and tectonic history between the northern and the intermediate block was first stressed by Borsi et al. (1973, 1978a) and Sassi et al. (1974). Along the Ahrn valley (Fig. 2), the Rb–Sr cooling ages of biotite (Borsi et al., 1973, 1978a) are about 300 Ma to the south, and about 28 Ma (Oligocene) to the north of the DAV (Fig. 2d). Furthermore, the Austroalpine basement to the north of the DAV, in marked contrast to the southern and the intermediate block, had already experienced intense deformation and upper greenschist facies metamorphism at an early stage of the Alpine history (Stöckhert, 1982). An early Cretaceous age for this early Alpine overprint is indicated by K–Ar cooling ages of ca. 100 Ma found in both preserved coarse-grained pre-Alpine pegmatitic muscovites and fine-grained phengites formed during the early Alpine metamorphism at 450 ± 50°C and 700 ± 150 MPa (Stöckhert, 1984). In the northern block, adjacent to the DAV, the early Alpine deformation was inhomogeneous. Consequently, the later Oligocene/Miocene overprint (discussed in this paper) affected structures and microstructures developed during the early Alpine overprint under upper greenschist facies conditions, or pre-Alpine fabrics in Variscan migmatites, that escaped the early Alpine overprint as nearly undeformed lenses with minor static retrogression.

Despite the dominant strike-slip character of the DAV, the contrast in biotite ages indicates a significant vertical component of displacement. This is consistent with a marked gradient in quartz microstructures across the DAV (Stöckhert, 1982; Kleinschrodt, 1987). The horizontal component of displacement is not well known. Geometric constraints (Ratschbacher et al., 1991) and rough estimates of shear strain (Kleinschrodt, 1987) suggest 20 ± 10 km as a rough estimate, accumulated within less than 10 m.y. between 35 and 25 Ma.

As the northern block cooled down during deformation, the cooling ages of biotite are interpreted to closely reflect the time of the tectonic activity, i.e. Oligocene. This is supported by the ages of ca. 30 Ma (Borsi et al., 1978b, 1979; Deutsch, 1984) found for magmatic intrusions (Rieserferner and Rensen plutons, numerous dikes and small intrusive bodies), whose emplacement interferes with the tectonic activity. A regional geotherm of about $30^{\circ}\mathrm{C\,km^{-1}}$ has been suggested for the Oligocene, based on the low grade metamorphic phase assemblages and the level of solidification of the contemporaneous magmatic intrusions (pressure ca. 300 MPa at ca. 300°C, Stöckhert, 1982; Trepmann and Stöckhert, in preparation). Based on this geotherm the temperatures can be correlated with depth as a first approximation.

3. New zircon fission track results

New low-temperature thermochronometric data provide the basis for the present analysis, complementing the extensive set of Rb–Sr biotite data provided by Borsi et al. (1973, 1978a), K–Ar ages of white mica by Stöckhert (1984), and fission track ages of apatite by Grundmann and Morteani (1985). The regional distribution of thermochronometric data within the area under consideration is displayed in Fig. 2(b–d), the locations of the new fission track samples are displayed in Fig. 2(a).

3.1. Analytical techniques

Between about 10 and 30 kg of suitable material was taken and processed in the usual manner: crushing, sieving, separation by Wilfley table and heavy liquids. Zircon populations for fission track analyses were prepared following the techniques outlined by Hurford et al. (1991). The zircons were embedded in FEP-Teflon, polished, and etched in a KOH–NaOH eutectic melt at about 214°C, with steps varying between 1 and 3 h, until a sufficient number of grains had been fully etched. Total etch time was 5–11 h. Thermal neutron irradiation was performed in the neutron facility R3 of the Risø National Research Centre at Roskilde/Denmark with a neutron fluence of $1\times10^{15}\,\mathrm{ncm^{-2}}$. The external detector method (Naeser, 1976; Gleadow, 1981) with a low uranium white mica detector was applied for the dating. The mica was etched for 45 min

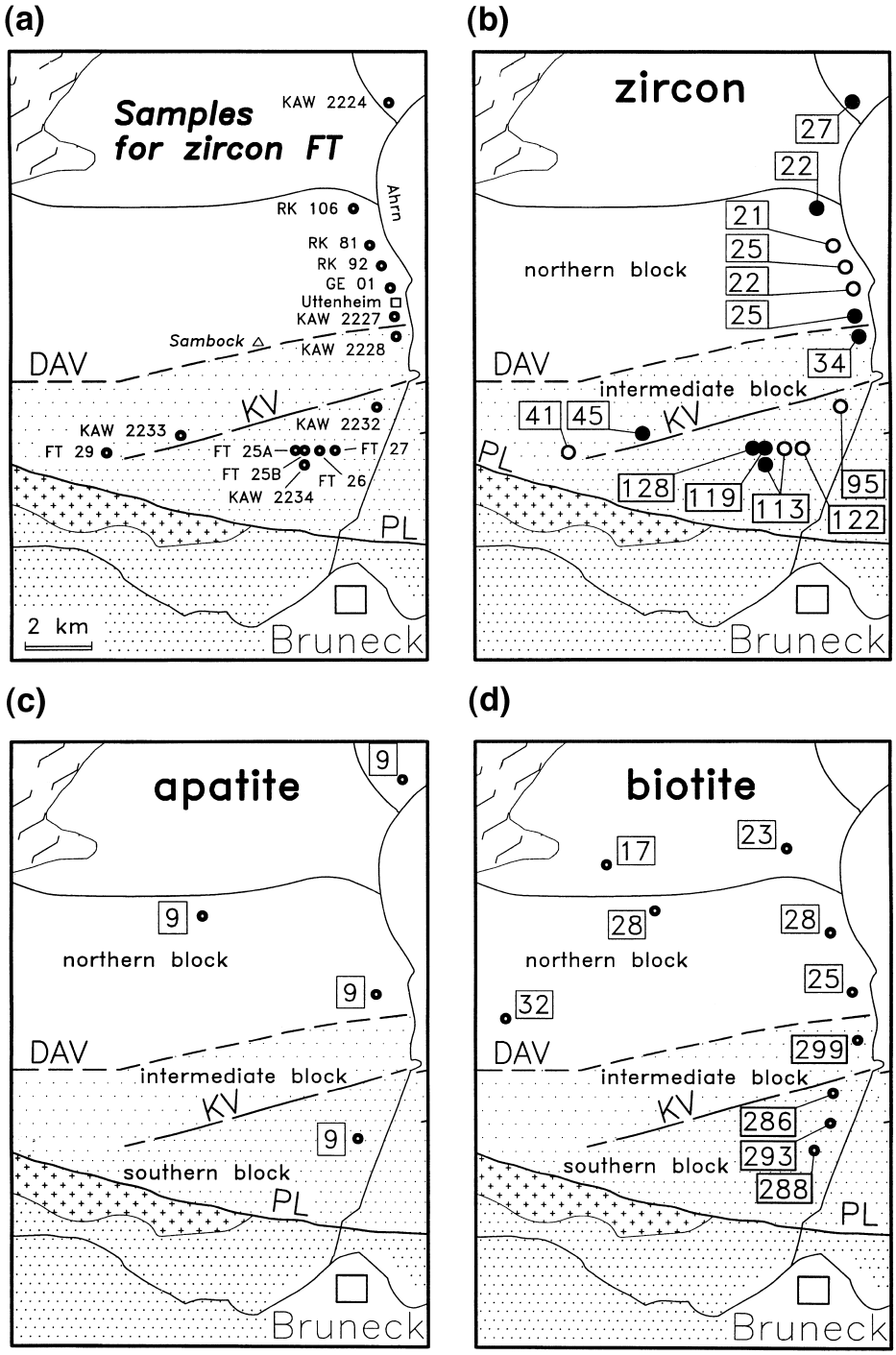

Fig. 2. Distribution of thermochronometric data in the studied area: (a) Sample locations of new zircon fission track data. (b) Fission track ages of zircon. Dots represent samples passing, and circles samples failing the χ^2-test (cf. Table 1). (c) Apatite fission track ages from Grundmann and Morteani (1985). (d) Rb–Sr biotite ages compiled from Borsi et al. (1973, 1978a,b).

in 40% HF at room temperature. Counting was performed on a ZEISS Axioplan microscope with a total magnification of 1250× using an oil immersion 100× objective. Ages were determined following the zeta approach (Hurford and Green, 1983). Calibration against CORNING CN-1 for MRB was established by repeated measurements on zircons from Fish Canyon Tuff, Buluk Member Tuff, Tardree Rhyolite, and Mount Dromedary Banatite age standards, resulting in a zeta of 117 ± 5 using the equipment of the London Fission Track Laboratory in 1990 and a zeta of 122 ± 5 for the equipment of the fission track labora-

Table 1
Zircon fission track data from the Ahrn valley section

Sample and locality	Mineral and number of crystals	Spontaneous		Induced		$P\chi^2$ (%)	$(\rho_s/\rho_i) \pm 1\sigma$	Dosimeter		Central age (Ma) $\pm 1\sigma$	Relative error (%)
		ρ_s	(N_s)	ρ_i	(N_i)			ρ_d	(N_d)		
FT 25A Kofl	zircon 20	162.60	(1998)	36.53	(449)	72	4.551 ± 0.261	4.778	(6598)	128.4 ± 6.9	0.6
FT 25B Kofl	zircon 20	217.40	(3063)	44.87	(632)	84	4.820 ± 0.194	4.070	(5621)	119.2 ± 5.5	0.4
FT 26 Kofl	zircon 20	160.20	(2699)	33.18	(559)	< 5	4.782 ± 0.282	4.070	(5621)	113.2 ± 7.6	19.3
FT 27 Kofl	zircon 20	143.70	(2580)	33.48	(601)	< 5	5.100 ± 0.339	4.778	(6598)	121.8 ± 7.9	18.1
FT 29 Moar	zircon 20	60.99	(758)	37.17	(462)	< 5	1.773 ± 0.146	4.070	(5621)	40.7 ± 3.3	23.3
GE 01 Uttenheim	zircon 20	43.11	(649)	49.23	(741)	< 5	0.963 ± 0.068	4.070	(5621)	22.2 ± 1.6	19.3
KAW 2224 Schloss Land	zircon 20	54.30	(1474)	36.80	(999)	39	1.522 ± 0.066	3.138	(3932)	27.0 ± 1.2†	5.3
KAW 2227 Uttenheim	zircon 20	47.92	(969)	34.77	(703)	89	1.430 ± 0.062	3.140	(3932)	25.3 ± 1.3†	0.7
KAW 2228 Spitzbach	zircon 14	40.98	(664)	20.36	(330)	99	2.043 ± 0.077	2.880	(3602)	33.8 ± 2.4†	0.0
KAW 2232 Gasthof Sonne	zircon 20	136.20	(2716)	26.37	(526)	< 5	5.571 ± 0.346	3.141	(3932)	94.9 ± 6.8†	22.4
KAW 2233 Platten	zircon 20	78.18	(1635)	31.70	(663)	59	2.393 ± 0.105	3.141	(3932)	45.0 ± 2.3†	4.4
KAW 2234 Ried	zircon 20	157.60	(1964)	25.35	(316)	78	6.622 ± 0.406	3.142	(3932)	113.2 ± 7.1†	0.1
RK 81 Griesberg	zircon 20	45.21	(793)	63.86	(1120)	< 5	0.773 ± 0.062	4.778	(6598)	21.0 ± 1.4	18.9
RK 92 Untergraber	zircon 5	44.52	(166)	42.64	(159)	< 5	1.101 ± 0.218	4.070	(5621)	25.2 ± 4.8	34.6
RK 106 Mühlen	zircon 20	44.95	(658)	60.32	(883)	34	0.775 ± 0.040	4.778	(6598)	21.7 ± 1.2	8.6

(1) Track densities (ρ) are in 10^5 tracks/cm^{-2}; numbers of tracks counted (N) shown in parentheses. (2) All analyses by external detector method using 0.5 for the $4\pi/2\pi$ geometry correction factor. (3) Ages calculated using dosimeter glass CN-1 and ζ-CN-1 = 122; for samples marked † ζ-CN-1 = 117. (4) $P\chi^2$ is the probability of obtaining χ^2 value for ν degrees of freedom where ν = no. of crystals − 1.

tory in Bochum from 1991 to 1996. Sample ages were calculated as central ages with 1σ errors (Galbraith and Laslett, 1993) and compiled in Table 1 according to the I.U.G.S. recommendations (Hurford, 1990).

3.2. Analytical results

The statistics in Table 1 show that the grain age distributions in some samples do not pass the χ^2-test and thus cannot be unequivocally attributed to a specific geological event. The increased spread in the grain ages probably results from various degrees of radiation damage in the analysed crystals. As the discordant samples occur in all three blocks with the ages fitting the general trend, we believe that this problem does not affect the conclusions drawn in the present paper. The regional distribution of the zircon fission track ages displayed in Fig. 2(c) clearly reveals three domains, corresponding to the three blocks. North of the DAV, the central ages fall in the range of 25 ± 4 Ma, being systematically below the biotite ages. A marked difference between sites to the east and to the west of the Ahrn valley is evident, which is also observed for the biotite data. To the west, the ages are in the range 23 ± 2 Ma, whereas the samples to the east of the valley yield 29 ± 2 Ma, suggesting displacement across a fault zone marked by the valley. The intermediate block, between the DAV and the KV, is characterized by scattering ages between 34 and 45 Ma. A sudden increase in ages occurs southwards across the KV, where ages cluster around 115 ± 20 Ma.

4. Thermal history

4.1. Closure temperatures

The interpretation of the thermochronometric data is based on the closure temperature concept (Dodson, 1973). For a given system, this closure temperature is a function of the cooling rate. It is also a function of specific properties, like mineral composition or defect structure (e.g. Harrison et al., 1985). Notwithstanding the fact that these influences are insufficiently specified, closure temperatures have been established for most geochronologic systems which appear to yield consistent results in most studies on natural systems (Hodges, 1991).

The generally accepted closure temperature for the K–Ar system of white mica ($T_{c\ \text{white mica K–Ar}}$) is in the range 350 ± 50°C (Purdy and Jäger, 1976). Lister and Baldwin (1996) quote 350–430°C. In the case of biotite, Purdy and Jäger (1976) suggested a closure temperature ($T_{c\ \text{biotite}}$) in the range 300 ± 50°C, identical for both the K–Ar and the Rb–Sr systems, based on their empirical study in the Central Alps. For a cooling rate of 10 K/m.y., Harrison et al. (1985) calculated a closure temperature slightly above 300°C (580 K) for the K–Ar system. The uncertainty may be of the order of ±30°C (Hodges, 1991). Lister and Baldwin (1996) suggest a somewhat higher closure temperature between 310 and 380°C for pressures between 0 and 10 kbar and cooling rates between 10 and 100°C/m.y. Here we use the value of 310 ± 30°C of Harrison et al. (1985) for discussion.

The closure temperature for fission tracks in zircon is less well established. Hurford (1986) originally proposed a closure temperature of 240 ± 50°C. This value is widely accepted and has led to reasonable results in different tectonic environments. Much of the more recent research, however, was concerned with a more precise definition of the limits of the partial annealing zone (PAZ). Based on annealing experiments and a fanning Arrhenius model, Yamada et al. (1996) propose a broad zircon partial annealing zone, between about 170 and 390 ± 25°C. Tagami and Shimada (1996) studying the contact metamorphic aureole of a granitic intrusion found a range from 230 to 330°C. For the low temperature limit of the PAZ, minimum values can be assessed from observations in deep drill holes, with Coyle and Wagner (1996) proposing 240°C, Green et al. (1996) 250°C, and Hejl et al. (1997) 260°C. The effective closure temperature, i.e. the temperature of the rock at the recorded fission track age, however, depends on a number of variables with radiation damage and cooling rate probably being the most important. A large number of studies (e.g. Hurford et al., 1991) show that the zircon fission track ages are systematically younger than the biotite ages from the same location. From calibrated cooling studies, Foster et al. (1996) propose a closure temperature of 260 ± 25°C. Correlation between thermobarometry (Theye et al., 1992) and zircon fission track ages in the high-pressure low-temperature metamorphic rocks of Crete, Greece, suggest that inferred temperatures of 300 ± 50°C were insufficient for significant annealing of the fission tracks in clastic zircon, whereas the fission track clock became completely reset in areas where geothermometry indicated 350 ± 50°C (Brix et al., in preparation). Considering the information actually available we prefer a closure temperature of 280 ± 30°C for radiation damaged crystals, which still matches the value given by Brandon and Vance (1992) for high cooling rates. This estimate may be subject to refinement, but—within the given limits of error—a future revision of the closure temperatures is not expected to significantly affect the conclusions drawn in the present paper.

Finally, the closure temperature for fission tracks in apatite is between about 100 and 120°C (see Wagner and Van den haute, 1992 for discussion), as recently reconfirmed in the KTB drill hole (Wagner et al., 1997).

4.2. Constraints on the thermal history

Based on the closure temperatures derived earlier, the regional distribution of the thermochronometric data (Fig. 2) reveals an internally consistent pattern. The major shear zones KV and DAV coincide with the boundaries between realms of different cooling histories. According to the apatite data of Grundmann and Morteani (1985), the late cooling history to below ca. 120°C is identical for the three blocks, indicating that no further vertical displacement along the KV and DAV took place when the rocks resided in the upper 4 km of the crust after about 10 Ma.

In the southern block, Carboniferous biotite ages are preserved and the fission track data on zircon scatter in the range 115 ± 15 Ma. This suggests that the Austroalpine basement exposed in the southern block had cooled down to below ca. 280 ± 30°C in the middle Cretaceous and remained between that temperature range and ca. 120°C throughout the Oligocene/Miocene tectonic activity.

The intermediate block—like the southern block—did not experience temperatures sufficient to reset the Variscan biotite ages during Alpine history. Some scatter (Fig. 2b) in the cooling ages reported by Borsi et al. (1978a,b) is presumably related to the intense deformation and partial decomposition of the biotites. The zircon fission track data—in marked contrast to those from the southern block—indicate that temperatures were still sufficient for track healing during the Eocene and cooling to below 280 ± 30°C occurred between about 45 and 35 Ma in the Ahrn valley cross-section. However, the considerable scatter of the zircon ages could also be taken as an indication that the intermediate block resided in the partial annealing zone for zircon at that time, or was even heated for a short period during tectonic activity. Shear heating, fluid transport facilitated by enhanced permeability, or heat transfer from the juxtaposed warmer levels of the northern block could possibly account for this. In any case, the zircon data preclude that the intermediate block was significantly above the closure temperature range for fission tracks in zircon at the time of displacement along the DAV in the Oligocene. We thus conclude that the temperatures were in the range 280 ± 30°C.

The northern block underwent intense early Alpine deformation and metamorphism prior to 100 Ma (K–Ar cooling ages of white mica; Stöckhert, 1984) and remained at temperatures above the closure temperature for the Rb–Sr and K–Ar systems of biotite, but below that for the K–Ar system of white mica into the Oligocene, i.e. between about 310 and 350°C, with the uncertainties discussed earlier. A temperature of ca. 330°C is therefore inferred for the northern block at the onset of the Oligocene deformation. Cooling to below the closure temperature of biotite took place in the late Oligocene, between about 30 and 25 Ma (Fig. 2d). The fission track ages of zircon (Fig. 2b) are systematically younger, but close to the biotite ages. This suggests rapid cooling during the tectonic activity along the DAV.

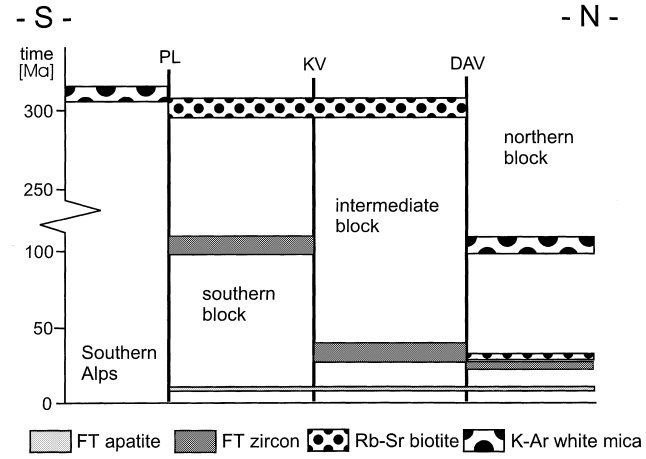

Fig. 3. The thermal history of the three blocks is reflected by the distribution of ages (Rb–Sr biotite ages from Borsi et al., 1973, 1978a,b; K–Ar white mica ages from Stöckhert, 1984, Hammerschmidt and Stöckhert, 1987; Apatite fission track ages from Grundmann and Morteani, 1985). Note that zircon fission track ages are close to, but systematically below the biotite ages in the northern block, and significantly below the biotite ages in the intermediate and the southern block. The age pattern across the DAV indicates that the largest portion of displacement took place within a few million years around 30 Ma, when the northern block was still above the closure temperature of biotite, whereas the intermediate block was around or just below the closure temperature for fission tracks in zircon.

The comparative cooling history for the three blocks is depicted in Fig. 3. A vertical displacement of about 1.5–2 km across the DAV can be estimated from the initial temperature contrast of ca. 50°C, using a thermal gradient of about 30°C km^{-1}, as proposed at that time by Stöckhert (1982).

5. Quartz microfabrics

The microfabrics of quartz developed during the Oligocene tectonic overprint are markedly distinct in the three blocks and reveal a continuous gradient across the DAV. In this section we first describe the characteristic optical microstructures of quartz (Fig. 4a–h) and the modification along a cross-section along the western flank of the Ahrn valley from south of the KV (southern block), through the intermediate block, to north of the DAV (northern block). The descriptions refer to pure quartz layers (deformed veins and segregations) where not otherwise specified. There is no contrast between quartz microstructures in the segregations and in their host rock. Five characteristic *c*-axis preferred orientation patterns along a 800 m section across the DAV are displayed in Fig. 5, together with recrystallized grain size and approximate proportion of recrystallized grains. Finally, the dislocation-microstructure of three samples taken along a section across the DAV is shown on representative transmission electron (TEM) micrographs together with the optical microstructure in Fig. 6(a–c).

5.1. Optical microstructures

5.1.1. Southern block

In the southern block, the pre-Alpine quartz microstructures are well preserved. In the amphibolite facies micaschists and gneisses the coarse quartz grains are mainly bound by phase boundaries. Grain size and shape are controlled by the distribution of the other minerals (Fig. 4a). Vein quartz reveals large grains with irregular shape. The superimposed slight to moderate low temperature plastic deformation, resulting in undulose extinction, is very weak in comparison to the intermediate block and could also have occurred during late Variscan exhumation. The microstructural record is interpreted to mean that Alpine deformation was localized into fault zones, whereas the volume of rock in the space between these faults remained essentially unaffected.

The transition from the brittle regime to that of distributed deformation in the intermediate block is not well exposed. It is likely that the southern block and the intermediate block (including the cataclasites related to the KV) were juxtaposed by displacement along a brittle fault zone after the stage of distributed deformation in the intermediate block, but still at temperatures above about 120°C, since there is no discontinuity in apatite fission track ages (Grundmann and Morteani, 1985).

5.1.2. Cataclasites of the KV

In the studied area, the KV is represented by a belt of cataclasites developed within granitic orthogneisses. Intense microfracturing and brecciation of feldspar and quartz is accompanied by dissolution and precipitation. Both the preserved original quartz grains and the quartz crystallized from the solution in pores and veinlets exhibits intense undulose extinction, kink and deformation bands, as well as basal deformation lamellae. The high angle grain boundaries are sutured with a very small wavelength and tiny new grains (5–10 μm) are formed at pre-existing high angle grain boundaries (Fig. 4b) and along deformation lamellae. Veinlets and filled vugs constitute a significant portion of the volume of the cataclasites. Fluid inclusions in quartz are abundant, mainly formed along healed fractures.

5.1.3. Intermediate block

In the intermediate block, quartz reveals intense plastic deformation. This deformation is highly inhomogeneous on the grain scale and depends on the crystallographic orientation. Locally, the orientation contrast between adjacent grains results in strongly

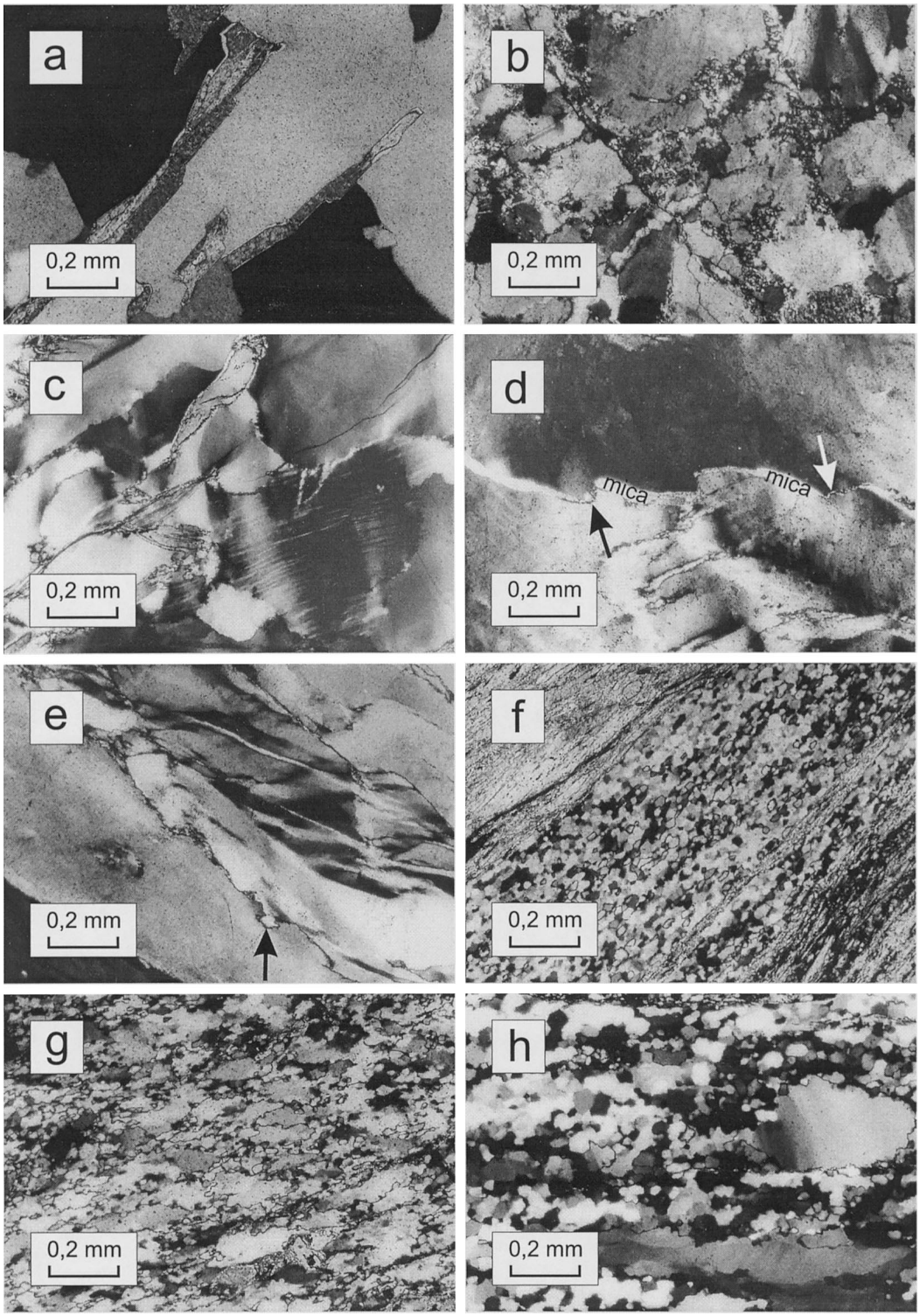

Fig. 4. Characteristic quartz microstructures (optical micrographs, crossed polarizers, long dimension 1.3 mm). (a) Southern block: pre-Alpine amphibolite facies quartz microstructures are preserved without any modification related to Alpine overprint. (b) KV cataclasites (derived from granitic orthogneiss): cataclastic deformation of feldspar and quartz; dissolution and precipitation. Crystal plastic deformation of quartz is indicated by pronounced undulose extinction and marginal migration recrystallization with a grain size <10 μm. (c) Intermediate block (paragneiss): quartz reveals intense undulose extinction, deformation bands and basal deformation lamellae. (d) Intermediate block (quartz vein): quartz shows intense undulose extinction; activity of pressure solution is indicated by formation of stylolitic mica seams (arrows). (e) Intermediate block (quartz vein): plastic deformation of quartz grains depends on crystallographic orientation; some grains show aspect ratios >5; recrystallization with a grain size between 5 and 10 μm is restricted to pre-existing high angle grain boundaries and deformation lamellae; migration recrystallization is conspicuous (arrow). (f) DAV mylonite (derived from the northern block): quartz is completely recrystallized with a grain size of about 20 μm. (g) Northern block, ca. 50 m north of the DAV: relic old quartz grains are polygonized; the sutured shape of the high angle grain boundaries and the aggregates of recrystallized grains with similar orientation suggest that both migration and rotation recrystallization were active during deformation by dislocation creep; recrystallized grain size is on the order of 20 μm. (h) Northern block, ca. 200 m north of the DAV: relic quartz grains are polygonized with low angle grain boundaries oriented parallel to the *c*-axis. Recrystallized grain size is on the order of 50 μm.

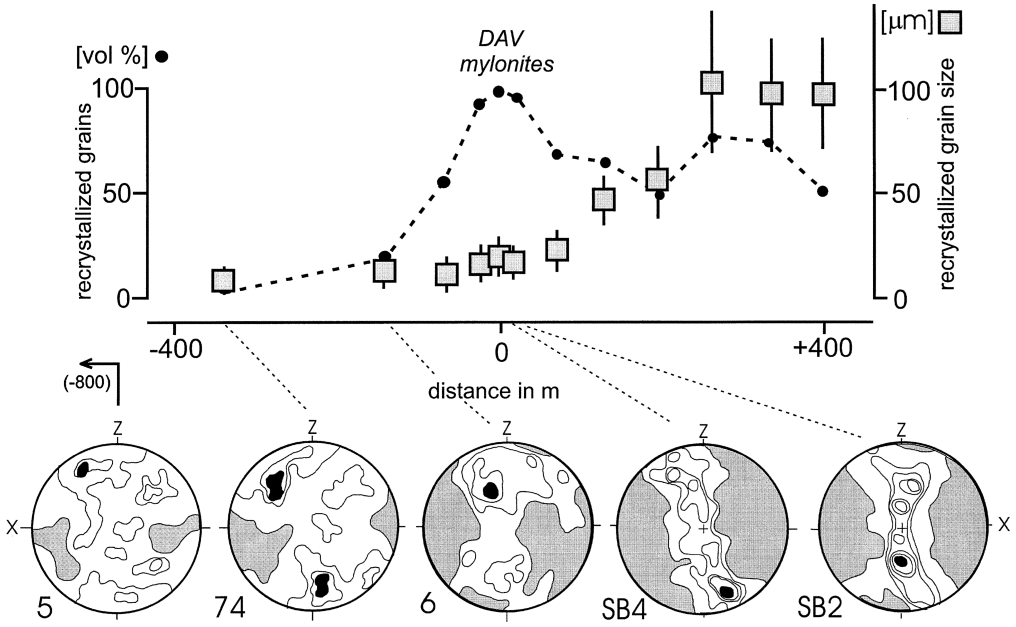

Fig. 5. Variation of recrystallized grain size, volume proportion of recrystallized grains, and lattice preferred orientation in pure quartz layers (former quartz veins) along an 800-m section across the DAV (location: crest and summit of Sambock mountain, 2396 m a.s.l., see Fig. 2a). Recrystallized grain size is given as the diameter of a circle with equal area. The error bars refer to the estimated ±30% uncertainty of these values, inherent to the irregular grain shape in three dimensions. Pole figures are lower hemisphere, equal area projections with contours of 2–4–6–8–10 per % total area.

distorted grains (Fig. 4c, e). In deformed quartz veins, crystals suitably oriented for glide on the basal plane reveal aspect ratios frequently exceeding a value of 10. Inhomogeneity of deformation is demonstrated by conspicuous deformation bands and kink bands (Fig. 4e). Deformation lamellae with basal orientation are very common (Fig. 4c). On the scale of the optical microscope, subgrain boundaries are poorly developed, if at all. High angle grain boundaries are sutured with a very small wavelength and tiny new grains with a diameter of ca. 5–10 μm are formed along pre-existing grain boundaries (Fig. 4e) or deformation lamellae. Abundant healed microfractures are marked by small fluid inclusions or visualized by faint contrasts under the cathodoluminescence microscope. Additionally, a high abundance of submicroscopic fluid inclusions is revealed by FTIR-spectrometry (Röller et al., in preparation).

The microstructures indicate distributed plastic deformation by dislocation glide. Recrystallization exclusively at pre-existing high angle grain boundaries or along deformation lamellae shows that grain boundary mobility is restricted to sites with pronounced lattice misorientation. Such migration recrystallization was reported by Hirth and Tullis (1992) on a much smaller scale in their regime 1, although the optical microstructure in the intermediate block is similar to that of their regime 2, apart from an apparently stronger dependence of grain scale strain on orientation. Likewise, in contrast to regime 2 as described by Hirth and Tullis (1992), the absence of well-ordered low-angle grain boundaries on both the optical and the TEM scale indicates that recovery by dislocation climb was less significant.

Within the gneisses, local concentration of deformation into mica layers is attributed to the low shear strength of mica. Experimental studies (Kronenberg et al., 1990; Shea and Kronenberg, 1992; Mares and Kronenberg, 1993) reveal that the shear strength of mica in favourable orientation is low compared to that of quartz at temperatures below about 300°C. In addition, dissolution of quartz enhanced along quartz–mica interfaces (e.g. Schwarz and Stöckhert, 1996) is inferred from structures resembling stylolites as shown in Fig. 4(d). The microstructures indicate that the partitioning of deformation due to simultaneous activation of dislocation glide, microcracking and pressure solution along interphase boundaries renders the mechanical behaviour of quartz in the field of semibrittle flow hard to predict from laboratory experiments. The behaviour of the bulk polyphase material is even more complex.

5.1.4. Mylonites of the DAV

High strain mylonitic rocks first appear about 800 m to the south of the DAV and their proportion increases significantly from about 400 m to the south of where the first unequivocal derivatives of the northern block with distinct lithology appear (DAV senso stricto in Fig. 5). A large portion of the banded mylo-

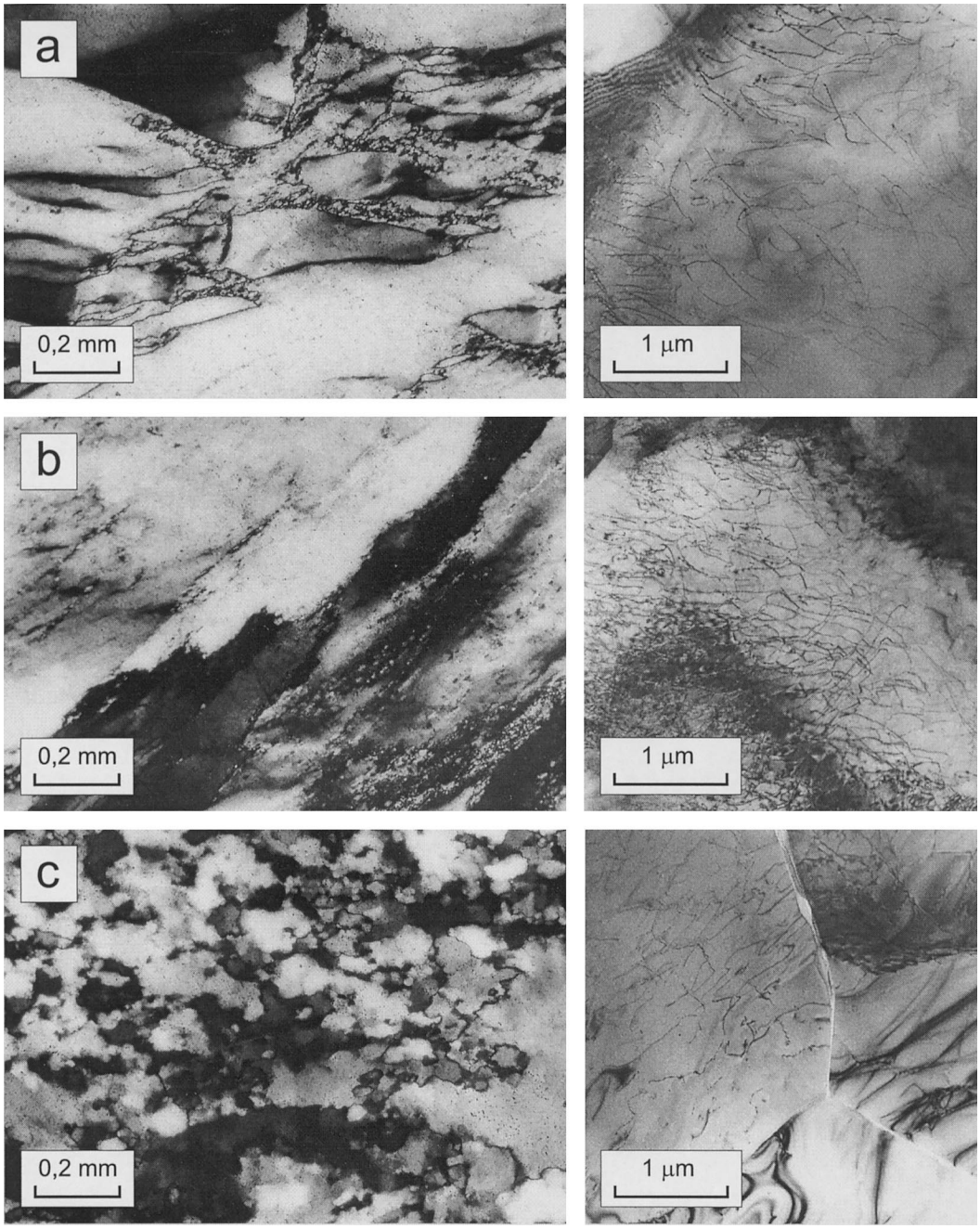

Fig. 6. Optical micrographs (left) and an example for TEM-scale microstructure (right) of samples PA10, PA4 and PA19, taken along a cross-section from the intermediate block into the DAV mylonites at the southern crest of the Sambock mountain (Fig. 2a). (a) Intermediate block, about 800 m south of the DAV: fairly homogeneous distribution of dislocations, poorly ordered dislocation walls with low misorientation. The free dislocation density is about $7\times10^{12}\,m^{-2}$. (b) Intermediate block, about 400 m south of DAV: Inhomogeneous distribution of dislocations with cellular walls and tangles. The average free dislocation density is about $2\times10^{13}\,m^{-2}$. (c) Mylonites of the DAV, sample derived from Northern Block: dislocation density varies between about 4 and $14\times10^{12}\,m^{-2}$, apparently due to a minor contrast between old and new grains. Voids along high angle grain boundaries may represent fluid inclusions.

nites consist of very fine-grained polyphase material, produced by retrogression of the original gneisses. In pure quartz layers, increasing grain shape strain correlates with an increasing portion of recrystallized grains, approaching 100% near the DAV s.s. (Fig. 4f), with a pronounced lattice preferred orientation (Fig. 5). The shape of the recrystallized grains in the pure quartz layers is nearly equant. The recrystallized grain size in the DAV mylonites amounts to about 10–20 μm (Figs. 4g and 5). The absence of a marked gradient in recrystallized grain size to the south of the DAV indicates that the flow stress was generally constant and the increase in finite strain over a few hundred metres towards the DAV is presumably a combined effect of

slightly increasing temperatures and strain softening. Strain softening in pure quartz layers (e.g. White et al., 1980; Tullis et al., 1990) can be caused by the increasing portion of recrystallized grains, concomitant grain size reduction, and geometrical softening due to development of the pronounced lattice preferred orientation (see Fig. 5).

5.1.5. Northern block

Our description here is restricted to the southernmost zone of the northern block (up to about 1 km N of the DAV). There, the structures and microstructures developed during the Oligocene deformation are superimposed on: (1) pre-Alpine migmatites which had undergone only minor static retrogression during the early Alpine metamorphism; and (2) strongly foliated rocks that had been formed from the same migmatites due to intense deformation under upper greenschist facies conditions during the early Alpine overprint, followed by grain growth of quartz (Stöckhert, 1982, 1984). Within ca. 1 km to the north of the DAV, both types of protoliths are highly strained and remnants of the originally mm-sized quartz grains are preserved as polygonized relics within a matrix of recrystallized grains (Fig. 4g, h). The low angle grain boundaries are generally oriented normal to (0001), giving rise to elongated subgrains parallel to the *c*-axis. In addition to subgrains, undulatory extinction is observed in the relic grains as well as—size permitting—in the recrystallized grains. The size of the recrystallized grains significantly increases towards the north from ca. 20 μm in the mylonites of the DAV to more than 50 μm a few hundred metres towards the north (Figs. 4g, h and 5). The shape of the larger recrystallized grains is elongate or irregular and sutured boundaries with wavelengths of less than 10 μm are observed (Fig. 6c). The *c*-axis preferred orientation is more pronounced than in the intermediate block (Fig. 5). The pattern remains consistent with ⟨*a*⟩ glide. Healed microcracks are significantly less abundant compared to the intermediate block. Finally, the microstructure of polyphase materials shows that quartz deforming by dislocation creep at the inferred temperature near 330°C reveals a very low effective viscosity compared to feldspar, mica and most other minerals, that all constitute nearly undeformed clasts.

The large clusters of recrystallized quartz grains with similar crystallographic orientation and intensely sutured high angle grain boundaries are invariably indicative of deformation by dislocation creep with both the rotation mechanism and the high-temperature migration mechanism being operative. Simultaneous effective recovery is revealed by well developed low-angle grain boundaries inside relic old grains. These features correspond to the regime 3 microstructure of Hirth and Tullis (1992). The larger recrystallized grains reveal sutured grain boundaries with a smaller wavelength and undulose extinction, or are partially replaced by smaller recrystallized grains. This is attributed to progressive deformation by dislocation creep under falling temperatures and increasing flow stress (also reflected by the dislocation microstructure, see later), with a rate of change not allowing for complete microstructural reequilibration (see Knipe, 1989; Prior et al., 1990).

5.2. Dislocation microstructure and dislocation density

The southernmost sample PA10 (Fig. 6a), situated in the intermediate block about 800 m to the south of the DAV, is characterized by a rather homogeneous distribution of dislocations and a uniform free dislocation density of about $7\times10^{12}\,m^{-2}$. Dislocation walls are poorly ordered and a rather wide spacing (about 100 nm) of geometrically necessary dislocations indicates slight misorientation across them. In contrast, the more strongly deformed sample PA4 (Fig. 6b), situated about 400 m to the south of the DAV, is characterized by a significantly higher free dislocation density of the order of $2\times10^{13}\,m^{-2}$ and an abundance of dislocation tangles surrounding cells with lower dislocation density. Well-ordered subgrain boundaries are not observed in the two samples from the intermediate block. Sample PA19 from the southern rim of the northern block, just to the north of the DAV (Fig. 6c) is completely recrystallized with a grain size of around 30 μm. On the TEM-scale, the distribution of dislocations is rather inhomogeneous. Dislocation tangles are observed aside of well ordered low-angle grain boundaries. The free dislocation density varies between 4×10^{12} and $2\times10^{13}\,m^{-2}$, partly reflecting the contrast across mobile high-angle grain boundaries, and partly presumably the inhomogeneous progressive deformation under falling temperatures.

5.3. Paleopiezometry

Recrystallized grain size, subgrain size, and free dislocation density of crystalline material deformed in the dislocation creep regime can be used as paleopiezometers to derive the flow stress if the following prerequisites are fulfilled: (1) steady-state dislocation creep has been achieved; (2) the microstructure has not been significantly modified during the subsequent geological history; and (3) an appropriate experimental or theoretical calibration is available. Principles and applications to quartz in natural rocks are discussed by Twiss (1977, 1986), Weathers et al. (1979), Kohlstedt and Weathers (1980), Christie and Ord (1980), Etheridge and Wilkie (1981) and Poirier (1985). Calibrations for quartz based on deformation experiments are subject to errors inherent to the experimen-

Table 2
Paleopiezometry (for microstructures and sample location cf. Fig. 6)

Sample	D [μm]	σ_T [MPa]	σ_M [MPa]	ρ	σ_W [MPa]
PA10	7	161	96	7×10^{12}	175
PA4	10	126	74	2×10^{13}	295
PA19	30	60	34	9×10^{12}	198

D = recrystallized grain size, ρ = dislocation density, σ = differential stress, subscript refers to calibration (T = Twiss, 1977; M = Mercier et al., 1977; W = Kohlstedt and Weathers, 1980).

tal techniques (Mercier et al., 1977; Gleason and Tullis, 1993). A theoretically derived calibration of the recrystallized grain size piezometer has been provided by Twiss (1977), one for dislocation density by Kohlstedt and Weathers (1980). High quality experimental data obtained by Gleason and Tullis (1993) are in accordance with the theoretical approach by Twiss (1977), which is preferred here. Although absolute errors may be large, orders of magnitude and relative changes of flow stress can be derived.

The results for samples PA10, PA4 and PA19 are given in Table 2. Based on the calibration of Twiss (1977), recrystallized grain size indicates decreasing flow stress from ca. 160 MPa, 800 m to the south of the DAV, over ca. 130 MPa, 400 m to the south of the DAV, to ca. 60 MPa and below in the southernmost part of the northern block. The stress estimates based on dislocation density (Kohlstedt and Weathers, 1980) correspond well to that derived from recrystallized grain size only for the southernmost sample, but are significantly higher in the northern block. There, the strain accumulated during the waning stage of deformation, with falling temperatures and increasing flow stress, was insufficient to cause an obliteration of the earlier microstructural record, which is still discernible on the optical scale, whereas on the TEM scale, high free dislocation densities reflect the late increase in flow stress.

5.4. Summary and comparison with experimentally established regimes

Whereas the quartz microstructures in the southern block indicate at best a faint plastic deformation in the low temperature plasticity regime, the microstructures from the KV onward towards the north are indicative of intense deformation in different subregimes of dislocation creep during the Oligocene. The marked gradient in the microstructures is correlated to both temperature and flow stress. A direct correlation with the microstructures developed in the three subregimes of dislocation creep proposed by Hirth and Tullis (1992), based on detailed microstructural analysis of experimentally deformed samples, appears to be not entirely satisfactory, however.

The quartz microstructures in the intermediate block compare favourably to regime 2 of Hirth and Tullis (1992), with strongly flattened original grains, abundant deformation lamellae and deformation bands, and a core and mantle structure. However, in contrast to the experimental observations of Hirth and Tullis (1992), migration recrystallization along pre-existing grain boundaries and deformation lamellae is dominant, and the absence of well-ordered subgrain boundaries on the TEM-scale is not consistent with effective recovery by dislocation climb. Overall, quartz deformation in the intermediate block involved a complex interplay of different deformation mechanisms, including dislocation glide, microcracking and pressure solution, difficult to resolve with respect to the bulk mechanical properties.

In the northern block, the optical-scale quartz microstructures developed in the earlier stages of deformation compare well to regime 3 of Hirth and Tullis (1992), with 'high temperature' migration recrystallization and recovery by dislocation climb both being active. In contrast, the dislocation microstructures partly resemble those observed in their regimes 1 and 2. This discrepancy is interpreted to reflect progressive deformation at falling temperatures and increasing flow stress. Stress relaxation and cooling were sufficiently fast to prevent complete obliteration of the earlier synkinematic microstructures. Also, indications of static polygonization or grain growth, commonly related to prolonged low stress annealing, are not discernible.

We believe that the observed discrepancies between the natural microstructural record and the characteristic features proposed by Hirth and Tullis (1992) for their three subregimes are accounted for by the following reasons. First, the microstructural record of natural samples is the integral of a long term deformation process, which is likely to have proceeded under changing conditions and subject to modification after the stage of interest. Unequivocal attribution of features to one and the same stage of deformation under a given set of boundary conditions may be impossible, in contrast to the quenched product of a deformation experiment. Second, the preservation potential of certain microstructures is low. This is particularly true for

microcracks which heal rapidly even at low temperatures (Smith and Evans, 1984). Third, the differential stress applied in the experimental studies of Hirth and Tullis (1992, 1994) exceeds the presumed natural level by up to one order of magnitude in subregime 1. Thus, the mechanisms and their combination need not be identical for both situations. For these reasons, a direct comparison between experimentally produced and natural microstructures should be made with great care, despite their apparent close similarity. This is particularly true for the low temperature/high stress range.

6. Discussion

6.1. Estimation of strain rate

In order to compare the natural microstructural record to predictions based on experimental flow laws, an estimate of strain rate is required in addition to information on temperature and flow stress. In most cases, geological strain rates have been inferred by combining finite strain with constraints on the time available to accumulate the strain (Pfiffner and Ramsay, 1982). This approach assumes that strain is accumulated continuously within the given time span, an assumption that need not be true. Higher strain rates would be encountered if deformation were episodic. In the present case episodic deformation cannot be excluded, but we do not see evidence to support this. Thus, like in most other case studies, only a rough estimation in accordance with geological boundary conditions and finite strain estimates is possible. For the sake of simplicity, we assume a horizontal displacement of 3 km by simple shear distributed over a 1-km-thick zone of the intermediate block (shear strain $\gamma \approx 3$), and another 20 km of displacement over a likewise 1-km-thick zone comprising the DAV mylonites and the southernmost part of the northern block (shear strain $\gamma \approx 20$). For a time span of 10 m.y., which is taken as an upper limit in view of the rapid changes in crustal configuration during collision (e.g. Ratschbacher et al., 1991), a strain rate on the order of $10^{-14}\,s^{-1}$ results for the intermediate block and $6\times10^{-14}\,s^{-1}$ for the DAV and southern rim of the northern block. If the movements took place within 1 m.y., the strain rates would be 10^{-13} and $6\times10^{-13}\,s^{-1}$. Strain rate estimates are rather insensitive to uncertainties in finite strain (see Pfiffner and Ramsay, 1982) and we believe that the obvious uncertainties in timing and displacement or strain are such that the uncertainty in strain rate does not exceed one order of magnitude, which is sufficient for the present purpose.

6.2. Comparison with experimentally derived flow laws

Various experimental techniques and starting materials have been used in experimental studies on dislocation creep of quartz aggregates, both 'dry' and 'wet' (compilations given in Carter and Tsenn, 1987, and Evans and Kohlstedt, 1995). Due to the abundance of aqueous fluid inclusions and the high concentration of water related defects in quartz, as revealed by FTIR microspectrometry (Röller et al., in preparation), only those studies referring to 'wet' conditions are considered here. However, the effect of water on the mechanical behaviour is still poorly understood and a generally accepted microphysical model is lacking. Evans and Kohlstedt (1995) and Post et al. (1996) have suggested that, for given flow stress and temperature, strain rate may be a function of water fugacity, with an exponent near one. In natural systems, water fugacity cannot easily be specified due to the complex composition of pore fluids and water activities <1. For shallow crustal positions the situation is additionally complicated by uncertainties on pore fluid pressure and time scales of equilibration.

Natural quartzites with added water were used for deformation experiments in a solid medium apparatus by Hansen and Carter (1982), Jaoul et al. (1984), Kronenberg and Tullis (1984), Koch et al. (1989), and Gleason and Tullis (1995). Using the molten salt cell technique, Gleason and Tullis (1995) obtained a stress exponent of 4, in contrast to the earlier studies with stress exponents, of well below 3, i.e. lower than predicted by theory. Synthetic quartzites produced from gel or silicic acid were used in the experiments performed by Paterson and Luan (1990) and Luan and Paterson (1992) in a gas medium apparatus at 300 MPa confining pressure. A compilation of flow law parameters derived by the various authors is presented in Table 3. Despite considerable scatter in the derived values for the activation energy Q and the stress exponent n, the majority of the quartz flow laws yield roughly consistent results. The flow law derived by Gleason and Tullis (1995) predicts the highest flow stresses for a given set of temperature and strain rate.

The flow stress–temperature relations predicted by the flow laws compiled in Table 3 for strain rates of 10^{-13} and $10^{-14}\,s^{-1}$ are shown in Fig. 7. The inferred temperatures for the intermediate and the northern block, and the flow stresses derived by the calibration of Twiss (1977) of the recrystallized grain size paleopiezometer are indicated. The decrease in flow stress from about 160 MPa in the intermediate block, over about 130 MPa in the mylonites proper, to below about 60 MPa in the adjacent part of the northern block is correlated with an increase in temperature from ca. 280°C to ca. 330°C (with an uncertainty of ca. $\pm$30°C). Fig. 7 demonstrates that these

Table 3
Power law parameters for wet quartzite

Reference	log A [(MPa)$^{-n}$ s^{-1}]	n	Q [kJ mol^{-1}]	Material	Remarks
H&C	−1.7	1.8	167	Simpson	α-qtz
K&T	−5.66	2.7	120	Heavitree	α-qtz
J	−2.54	1.8	151	Heavitree	α-qtz
K	−5.94	2.7	134	Simpson	α-qtz
L&P	−7.18	3.1	135	synth. (gel)	β-qtz
L&P	−9.40	4.0	135	synth. (acid)	β-qtz

Flow law: $\varepsilon = A \exp(-Q/RT)\sigma^{-n}$. References: H&C = Hansen and Carter (1982), K&T = Kronenberg and Tullis (1984), J = Jaoul et al. (1984), K = Koch et al. (1989), L&P = Paterson and Luan (1990), Luan and Paterson (1992).

stress–temperature pairs compare well to those predicted by flow laws for wet quartzite extrapolated to natural strain rates of between about 10^{-13} and 10^{-14} s^{-1}. Also, it is evident that the uncertainty in strain rate of one order of magnitude corresponds approximately to the uncertainty inherent in thermometry and, thus, does not significantly affect the conclusions drawn in this paper. Despite remaining uncertainties, this consistency between natural record and experimental flow laws suggests that extrapolation of laboratory data to natural strain rates are justified and that models based on these extrapolations are realistic.

6.3. A comparison with findings from the KTB drill hole

Access to the brittle–ductile transition was a major goal of the KTB deep drill hole in eastern Bavaria, Germany, that reached 9101 m depth and ca. 265°C, i.e. conditions close to those inferred for the intermediate block. In the KTB, differential stress as a function of depth has been estimated from a combination of methods, including several hydrofracture experiments (Brudy et al., 1997; Zoback and Harjes, 1997). Hydrostatic pore fluid pressures were recorded down to 9 km (Grawinkel and Stöckhert, 1997; Huenges et al., 1997). The microstructural record of quartz has been studied by Dresen et al. (1997). The free dislocation densities of quartz at 9 km depth and 265°C amount to about 1×10^{13} m^{-2} and indicate a differential stress on the order of 140 MPa using the calibration of Kohlstedt and Weathers (1980), whereas extrapolation of the in-situ stress measurements to 9 km suggests a higher differential stress between about 170 and 220 MPa, depending on the friction coefficient assumed for fault planes. Although the magnitude of differential stress compares well to that derived for the intermediate block, the optical microstructures related to deformation of quartz in the semibrittle regime are much less developed and the strain accumulated in the anorogenic intraplate setting over the past 60 m.y. (Wagner et al., 1997) is negligible. These findings suggest that the temperatures during the Oligocene deformation in the intermediate block significantly exceeded the value of 265°C, allowing for a high strain rate when compared to the KTB situation.

6.4. Implications for the brittle–ductile and the brittle–plastic transition

Three rheological regimes have been proposed for crustal material, as a function of confining pressure and temperature from top to bottom: brittle, semibrittle and plastic (Evans and Kohlstedt, 1995; Kohlstedt et al., 1995). The transition between the brittle and the semibrittle regime is referred to as the 'brittle–ductile transition' (BDT), and the transition between the semibrittle and the plastic regime as the 'brittle–plastic transition' (BPT). The BDT is defined as the change from localized to distributed failure, and the BPT that from distributed brittle failure to pressure insensitive purely crystal plastic flow.

In terms of these rheological regimes, the southern block represents the regime of localized brittle failure. During the Oligocene tectonic evolution it represents the upper crust, more shallow than the BDT. The intermediate block represents the semibrittle regime characterized by non-localized ductile flow. In this regime between the BDT and BPT, high-stress dislocation creep of quartz is accompanied by microcracking and pressure solution. Finally, the earlier stage of deformation in the northern block represents steady-state dislocation creep of quartz at moderate stress in the fully plastic regime beneath the BPT, the microstructures being partially overprinted by cooling during progressive deformation.

Evans and Kohlstedt (1995) and Kohlstedt et al. (1995) suggest that the BPT is reached when the effective confining pressure equals the flow strength of the material (Goetze's criterion). For a natural geological situation, the effective mean stress $(\sigma_1 + \sigma_2 + \sigma_3)/3$ is

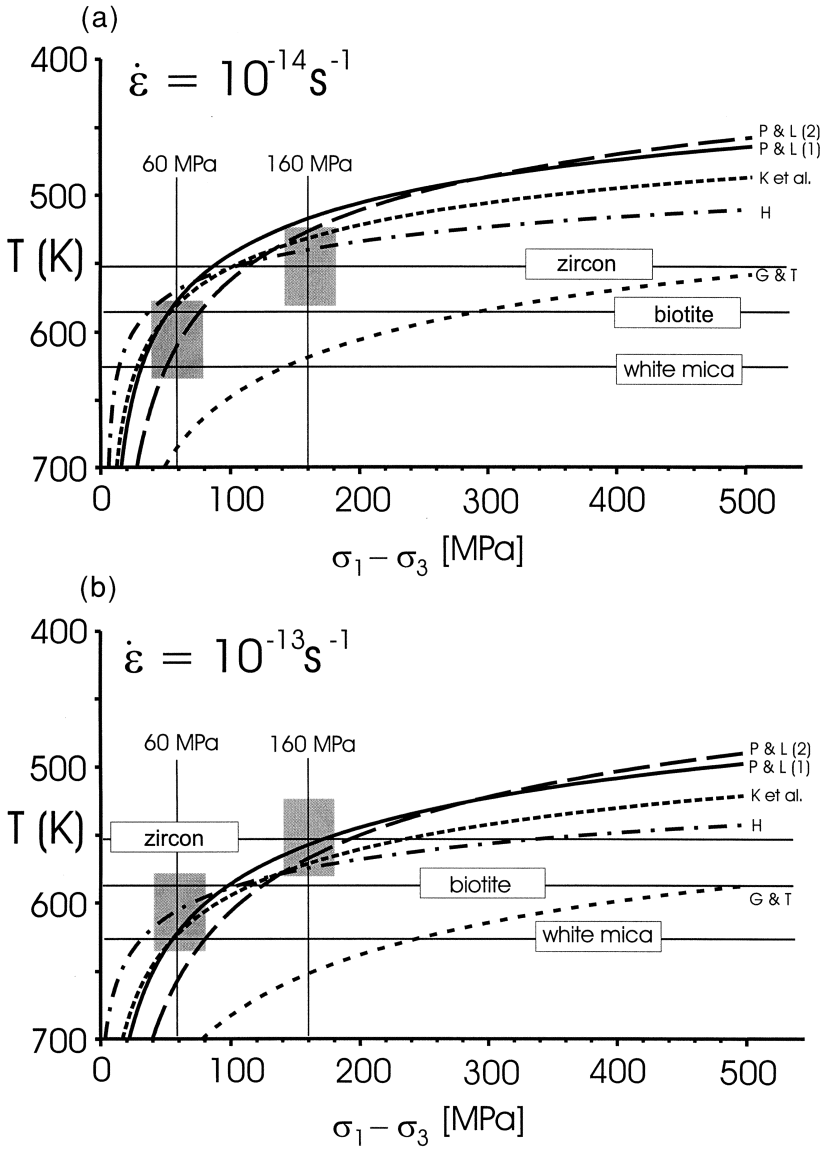

Fig. 7. Experimentally derived flow laws for dislocation creep of wet quartz (P&L (1): Paterson and Luan, 1990, 'best choice 1'; P&L (2): Paterson and Luan, 1990, 'best choice 2'; K et al.: Koch et al., 1989; H: Hansen and Carter, 1982; G&T: Gleason and Tullis, 1995) displayed in flow stress vs temperature diagrams for a constant strain rate of (a) $10^{-14}\,s^{-1}$ and (b) $10^{-13}\,s^{-1}$. The closure temperatures for K–Ar of white mica, Rb–Sr and K–Ar of biotite, and fission tracks in zircon are indicated (see text for discussion). Vertical lines indicate the flow stresses derived by the recrystallized grain size paleopiezometer (Twiss, 1977; see Table 2) for the intermediate block and the southernmost rim of the northern block. The respective combinations (280°C/160 MPa for the intermediate and 330°C/60 MPa for the northern block) are visualized by the shaded boxes. For these conditions most flow laws predict strain rates on the order of 10^{-13}–$10^{-14}\,s^{-1}$. See text for discussion.

taken as being equivalent to the effective confining pressure. In a strike-slip regime with $\sigma_2 = \sigma_v$ it can be approximated by the effective overburden stress σ_{veff} for simplicity. The thermal constraints combined with the inferred geotherm near $30°C\,km^{-1}$ allow the testing of the prediction of Goetze's criterion for the BPT across the DAV. Initial temperatures of 270°C (for discussion) in the intermediate block and 330°C in the northern block correspond to depths of 9, and respectively, 11 km. For an average rock density of $2650\,kg\,m^{-3}$, the lithostatic pressure (σ_v) at these depths is given as 234 and 286 MPa. For a hydrostatic pore fluid pressure and an average fluid density of $1000\,kg\,m^{-3}$, the effective overburden stress (σ_v–p_{fluid}) would be reduced to 146 MPa at 9 km depth in the intermediate block, and to 178 MPa at 11 km in the northern block. However, it is questionable whether a hydrostatic pore fluid pressure can also be assumed for the conditions prevailing beneath the BPT (e.g. Brace, 1980; Fournier, 1991) and hence 178 MPa only form an upper bound. For the intermediate block, the recrystallized grain size paleopiezometer (Twiss, 1977)

yields a differential stress of ca. 160 MPa (Table 2), i.e. higher than the effective overburden stress at hydrostatic pore fluid pressure, whereas only 60 MPa are indicated for the northern block, which remains below the effective overburden stress for pore fluid pressures of up to 80% of the vertical normal stress. Thus, the inferred conditions at the BPT are consistent with the prediction by Goetze's criterion.

7. Conclusions

The microstructural record of quartz along the investigated cross-section reflects deformation in different rheological regimes during a relatively short-lived period of tectonic activity in the Oligocene. Oblique strike-slip displacement has juxtaposed blocks with contrasting mechanical behaviour. The thermochronometric constraints, based on published mica ages and new fission track data of zircon, indicate that the transition between these regimes was controlled by temperature and that the initial contrast in temperature between the intermediate and the northern block amounted to about 50°C. For the derived temperature/flow stress combinations, the majority of available experimental flow laws for dislocation creep of wet quartzite predict strain rates on the order of 10^{-13}–$10^{-14}\,s^{-1}$, consistent with the geological constraints. This supports the validity of the extrapolation of the experimental data to natural strain rates.

The data confirm that—under the given conditions and for strain rates on the order of 10^{-13}–$10^{-14}\,s^{-1}$ that are presumably characteristic for an active collisional orogenic belt—localized brittle deformation is restricted to temperatures well below the closure temperature for fission tracks in zircon. Distributed ductile deformation in the semibrittle regime between the BDT and the BPT, with simultaneous activity of high-stress dislocation creep of quartz, microcracking and pressure solution, proceeds at temperatures near the closure temperature for fission tracks in zircon, which we estimate to be about 280 ± 30°C. Steady state dislocation creep of quartz at moderate stress in the fully plastic regime, i.e. beneath the brittle–plastic transition, is effective at temperatures above the closure temperature for K–Ar and Rb–Sr of biotite (ca. 310 ± 30°C), but well below that for the K–Ar-system of white mica (ca. 350 ± 50°C). Thus, the BPT for quartz approximately coincides with the closure temperature for biotite. The microstructures reveal that at this temperature quartz becomes the phase with the lowest flow strength, compared to feldspar and mica, and thus controls the rheology of quartz-rich continental material until eventually superseded by feldspar at temperatures above ca. 500°C (Voll, 1976; Tullis, 1983; Simpson, 1985).

The temperature range derived for the BPT approximately coincides with that inferred for the lower bound for continental intraplate seismicity (e.g. Meissner and Strehlau, 1982; Chen and Molnar, 1983; Scholz, 1990), subject to the validity of thermal models. The internal consistency between predictions based on three completely independent approaches, i.e. the observed depth distribution of intracontinental seismicity, the extrapolation of laboratory data to natural strain rates, and the correlation between thermobarometry and microstructural record in exhumed natural rocks appears very promising and in particular supports the validity of rheologic models based on the extrapolations of experimentally derived flow laws.

Acknowledgements

The microstructural observations and principal conclusions drawn in this paper date back to the period when B.S. and R.K were graduate students at Erlangen under supervision of Günter Nollau. To him our sincere thanks for all he gave to us. Frank Hansen is thanked for the mineral separation, Friedrich Eickhoff for the careful preparation of thin sections, Karin Aschenbrenner and Michael Ress for the processing of the photographs. The zircon fission track dating was performed under the EU-contract SC1*-0453(JR). Stuart Thomson is thanked for kindly correcting the English. Jörg Renner, Johannes Duyster and Martina Küster are thanked for commenting on early drafts of the manuscript. Careful and constructive reviews by Jan Tullis and Mark Brandon significantly improved the paper and are gratefully acknowledged.

References

Bianchi, A., 1934. Studi petrografici sull'Alto Adige Orientale e regione limitrofe. Memoriae Istituto Geologia Universid Padova X (5), 243.

Bigi, G., Cosentino, D., Parotto, M., Sartori, R., Scandone, P., 1973. Structural Model of Italy, Consiglio Nazionale della Richerche, Roma.

Borsi, S., Del Moro, A., Sassi, F.P., Zirpoli, G., 1973. Metamorphic evolution of the Austridic rocks to the south of the Tauern Window (Eastern Alps): radiometric and geopetrologic data. Memorie della Società Geologica Italiana 12, 549–571.

Borsi, S., Del Moro, A., Sassi, F.P., Zanferrari, A., Zirpoli, G., 1978a. New geopetrologic and radiometric data on the Alpine history of the Austridic continental margin south of the Tauern Window. Memorie degli Istituti di Geologia e Mineralogia dell'Universitá di Padova 32, 17.

Borsi, S., Del Moro, A., Sassi, F.P., Zirpoli, G., 1978b. On the age of the periadriatic Rensen massiv (Eastern Alps). Neues Jahrbuch für Geologie und Paläontologie, Monatshefte 267–272.

Borsi, S., Del Moro, A., Sassi, F.P., Zirpoli, G., 1979. On the age of the Vedrette di Ries (Rieserferner) massif and its geodynamic signifi-

cance. Neues Jahrbuch für Geologie und Paläontologie, Monatshefte 41–60.
Brace, W.F., 1980. Permeability of crystalline and argillaceous rocks. International Journal of Rock Mechanics, Mineral Sciences and Geomechanics Abstract Volume 17, 241–251.
Brace, W.F., Kohlstedt, D.L., 1980. Limits on lithospheric stress imposed by laboratory experiments. Journal of Geophysical Research 85, 6248–6252.
Brandon, M.T., Vance, J.A., 1992. Tectonic evolution of the Cenozoic Olympic subduction complex, Washington State, as deduced from fission track ages for detrital zircons. American Journal of Science 292, 565–636.
Brudy, M., Zoback, M.D., Fuchs, K., Rummel, F., Baumgärtner, J., 1997. Estimation of the complete stress tensor to 8 km depth in the KTB scientific drill holes: Implications for crustal strength. Journal of Geophysical Research 102, 18,453–18,475.
Carter, N.L., Tsenn, M.C., 1987. Flow properties of continental lithosphere. Tectonophysics 136, 27–63.
Chen, W.P., Molnar, P., 1983. Focal depths of intracontinental and intraplate earthquakes and their implications for the thermal and mechanical properties of the lithosphere. Journal of Geophysical Research 88, 4183–4214.
Christie, J.M., Ord, A., 1980. Flow stress from microstructures of mylonites: example and current assessment. Journal of Geophysical Research 85, 6253–6262.
Coward, M., Dietrich, D., 1989. Alpine tectonics—an overview. In: Coward, M.P., Dietrich, D., Park, R.G. (Eds.), Alpine Tectonics. Geological Society, London, Special Publication 45, pp. 1–29.
Coyle, D.A., Wagner, G.A., 1996. Fission-track dating of zircon and titanite from the 9101 m deep KTB: Observed fundamentals of track stability and thermal history reconstruction. International Workshop on Fission-Track Dating, Gent, Abstr., 22.
Dal Piaz, G., 1934. Studi geologici sull'Alto Adige Orientale e regione limitrofe. Memorie degli Istituti di Geologia e Mineralogia dell'Universitá di Padova X, 1–238.
Deutsch, A., 1984. Young Alpine dykes south of the Tauern Window (Austria): A K–Ar and Sr isotope study. Contributions to Mineralogy and Petrology 85, 45–57.
Dietrich, V.J., 1976. Plattentektonik in den Ostalpen, Eine Arbeitshypothese. Geotektonische Forschungen 50, 1–84.
Dodson, M.H., 1973. Closure temperature in cooling geochronological and petrological systems. Contributions to Mineralogy and Petrology 40, 259–274.
Dresen, G., Duyster, J., Stöckhert, B., Wirth, R., Zulauf, G., 1997. Quartz dislocation microstructure between 7000 m and 9100 m depth from the Continental Deep Drilling Project KTB. Journal of Geophysical Research 102, 18,443–18,452.
Dunlap, W.J., Hirth, G., Teyssier, C., 1997. Thermomechanical evolution of a ductile duplex. Tectonics 16, 983–1000.
Etheridge, M.A., Wilkie, J.C., 1981. An assessment of dynamically recrystallized grainsize as a palaeopiezometer in quartz-bearing mylonite zones. Tectonophysics 78, 475–508.
Evans, B., Kohlstedt, D.L., 1995. Rheology of rocks. In: Ahrens, T.J. (Ed.), Rock Physics & Phase Relations—A Handbook of Physical Constants. American Geophysical Union, Washington, pp. 148–165.
Foster, D.A., Gleadow, A.J.W., Noble, W.P., 1996. Sphene and zircon fission track closure temperatures revisited: Empirical calibrations from $^{40}Ar/^{39}Ar$ diffusion studies of K-feldspar and biotite. International Workshop on Fission-Track Dating, Gent, Abstr., 37.
Fournier, R.O., 1991. The transition from hydrostatic to greater than hydrostatic fluid pressure in presently active continental hydrothermal systems in crystalline rock. Geophysical Research Letters 18, 955–958.
Frisch, W., 1976. Ein Modell zur alpidischen Evolution und Orogenese des Tauernfensters. Geologische Rundschau 65, 375–392.
Frisch, W., 1979. Tectonic progradation and plate tectonic evolution of the Alps. Tectonophysics 60, 121–139.
Galbraith, R.F., Laslett, G.M., 1993. Statistical models for mixed fission track ages. Nuclear Tracks Radiation Measurements 21, 459–470.
Gleadow, A.J.W., 1981. Fission track dating: what are the real alternatives. Nuclear Tracks 5, 3–14.
Gleason, G.C., Tullis, J., 1993. Improving flow laws and piezometers for quartz and feldspar aggregates. Geophysical Research Letters 20, 2111–2114.
Gleason, G.C., Tullis, J., 1995. A flow law for dislocation creep of quartz aggregates determined with the molten salt cell. Tectonophysics 247, 1–23.
Goetze, C., Evans, B., 1979. Stress and temperature in the bending lithosphere as constrained by experimental rock mechanics. Geophysical Journal Royal Astronomical Society 59, 463–478.
Grawinkel, A., Stöckhert, B., 1997. Hydrostatic pore fluid pressure to 9 km depth—Fluid inclusion evidence from the KTB deep drill hole. Geophysical Research Letters 24, 3273–3276.
Green, P.F., Hegarty, K.A., Duddy, I.R., Foland, S.S., Gorbachev, V., 1996. Geological constraints on fission track annealing in zircon. International Workshop on Fission-Track Dating, Gent, Abstr., 44.
Grundmann, G., Morteani, G., 1985. The young uplift and thermal history of the central eastern Alps (Austria/Italy), evidence from apatite fission track ages. Jahrbuch Geologische Bundesanstalt Wien 128, 197–216.
Hammerschmidt, K., Stöckhert, B., 1987. A K–Ar and $^{40}Ar/^{39}Ar$ study on white micas from the Brixen Quartzphyllite, Southern Alps. Evidence for argon loss at low temperatures. Contributions to Mineralogy and Petrology 95, 393–406.
Hansen, F.D., Carter, N.L., 1982. Creep of selected crustal rocks at 1000 MPa. EOS Transactions American Geophysical Union 63, 437 (abstr.).
Harrison, T.M., Duncan, I., McDougall, I., 1985. Diffusion of ^{40}Ar in biotite: temperature, pressure and compositional effects. Geochimica Cosmochimica Acta 49, 2461–2468.
Hejl, E., Coyle, D., Lal, N., Van den Houte, P., Wagner, G.A., 1997. Fission-track dating of the western border of the Bohemian massif: thermochronology and tectonic implications. Geologische Rundschau 86, 210–219.
Hirth, G., Tullis, J., 1992. Dislocation creep regimes in quartz aggregates. Journal of Structural Geology 14, 145–159.
Hirth, G., Tullis, J., 1994. The brittle–plastic transition in experimentally deformed quartz aggregates. Journal of Geophysical Research 99, 11731–11747.
Hodges, K.V., 1991. Pressure–temperature–time paths. Annual Reviews Earth and Planetary Sciences 19, 207–236.
Hofmann, K.-H., Kleinschrodt, R., Lippert, R., Mager, D., Stöckhert, B., 1983. Geologische Karte des Altkristallins südlich des Tauernfensters zwischen Pfunderer Tal und Tauferer Tal, Südtirol. Der Schlern 57, 572–590.
Huenges, E., Erzinger, J., Kück, J., Engeser, B., Kessels, W., 1997. The permeable crust: geohydraulic properties down to 9100 m depth. Journal of Geophysical Research 102, 18,255–18,265.
Hurford, A.J., 1986. Cooling and uplift patterns in the Lepontine Alps south central Switzerland and an age of vertical movement on the Insubric fault line. Contributions to Mineralogy and Petrology 92, 413–427.
Hurford, A.J., 1990. Standardization of fission track dating calibration: Recommendation by the Fission Track Working Group of the I.U.G.S. Subcommission on Geochronology. Chemical Geology (Isotope Geoscience Section) 80, 171–178.
Hurford, A.J., Green, P.F., 1983. The zeta age calibration of fission-track dating. Isotope Geoscience 1, 85–317.
Hurford, A.J., Hunziker, J.C., Stöckhert, B., 1991. Constraints on the late thermotectonic evolution of the western Alps: evidence for episodic rapid uplift. Tectonics 10, 758–769.

Jaoul, O., Tullis, J., Kronenberg, A., 1984. The effect of varying water contents on the creep behavior of Heavitree quartzite. Journal of Geophysical Research 89, 4298–4312.

Kleinschrodt, R., 1987. Quarzkorn-Gefügeanalyse im Altkristallin südlich des westlichen Tauernfensters (Südtirol/Italien). Erlanger Geologische Abhandlungen 114, 1–82.

Knipe, R.J., 1989. Deformation mechanisms—recognition from natural tectonites. Journal of Structural Geology 11, 127–146.

Koch, P.S., Christie, J.M., Ord, A., George, R.P., Jr, 1989. Effect of water on the rheology of experimentally deformed quartzite. Journal of Geophysical Research 94, 13,975–13,996.

Kohlstedt, D.L., Weathers, M.S., 1980. Deformation induced microstructures, paleopiezometers, and differential stresses in deeply eroded fault zones. Journal of Geophysical Research 85, 6269–6285.

Kohlstedt, D.L., Evans, B., Mackwell, S.J., 1995. Strength of the lithosphere: Constraints imposed by laboratory experiments. Journal of Geophysical Research 100, 17,587–17,602.

Kronenberg, A.K., Tullis, J., 1984. Flow strengths of quartz aggregates: grain size and pressure effects due to hydrolytic weakening. Journal of Geophysical Research 89, 4281–4297.

Kronenberg, A.K., Kirby, S.H., Pinkston, J., 1990. Basal slip and mechanical anisotropy of biotite. Journal of Geophysical Research 95, 19,257–19,278.

Lister, G.S., Baldwin, S.L., 1996. Modelling the effect of arbitrary *P–T–t* histories on argon diffusion in minerals using the MacArgon program for the Apple Macintosh. Tectonophysics 253, 83–109.

Luan, F.C., Paterson, M.S., 1992. Preparation and deformation of synthetic aggregates of quartz. Journal of Geophysical Research 97, 301–344.

Mares, V.M., Kronenberg, A.K., 1993. Experimental deformation of muscovite. Journal of Structural Geology 15, 1061–1075.

Meissner, R., Strehlau, J., 1982. Limits of stresses in continental crusts and their relation to the depth–frequency distribution of shallow earthquakes. Tectonics 1, 73–89.

Mercier, J.-C.C., Anderson, D.A., Carter, N.L., 1977. Stress in the lithosphere: inferences from steady-state flow of rocks. Journal of Pure and Applied Geophysics 115, 199–226.

Naeser, C.W., 1976. Fission-track dating. U.S. Geological Survey Open-File Report 76-190.

Paterson, M.S., 1987. Problems in the extrapolation of laboratory rheological data. Tectonophysics 133, 33–43.

Paterson, M.S., Luan, F.C., 1990. Quartzite rheology under geological conditions. In: Knipe, R.J., Rutter, E.H. (Eds.), Deformation Mechanisms, Rheology and Tectonics. Geological Society, London, Special Publication 54, pp. 299–307.

Pfiffner, O.A., Ramsay, J.G., 1982. Constraints in geological strain rates: arguments from finite-strain states of naturally deformed rocks. Journal of Geophysical Research 87, 311–321.

Poirier, J.-P., 1985. Creep of Crystals—High-temperature Deformation Processes in Metals, Ceramics and Minerals. Cambridge University Press, Cambridge.

Post, A.D., Tullis, J., Yund, R.A., 1996. Effects of chemical environment on dislocation creep of quartzite. Journal of Geophysical Research 101, 22,143–22,155.

Prior, D.J., Knipe, R.J., Handy, M.R., 1990. Estimates of the rates of microstructural changes in mylonites. In: Knipe, R.J., Rutter, E.H. (Eds.), Deformation Mechanisms, Rheology and Tectonics. Geological Society, London, Special Publication 54, pp. 309–319.

Purdy, J.W., Jäger, E., 1976. K–Ar ages on rock-forming minerals from the Central Alps. Memorie degli Istituti di Geologia e Mineralogia dell'Universitá di Padova 30, 1–34.

Ranalli, G., Murphy, D.C., 1987. Rheological stratification of the lithosphere. Tectonophysics 132, 281–295.

Ratschbacher, L., Frisch, W., Linzer, H.-G., Merle, O., 1991. Lateral extrusion in the eastern Alps, part 2: structural analysis. Tectonics 10, 257–271.

Sassi, F.P., Zanferrari, A., Zirpoli, G., 1974. Some considerations on the South-Alpine basement of the Eastern Alps. Neues Jahrbuch für Geologie und Paläontologie, Monatshefte 609–624.

Schmid, S.M., 1982. Microfabric studies as indicators of deformation mechanisms and flow laws operative in mountain building. In: Hsü, K.J. (Ed.), Mountain Building Processes. Academic Press, London, pp. 95–110.

Scholz, C.H., 1990. The Mechanics of Earthquakes and Faulting. Cambridge University Press, Cambridge.

Schulz, B., 1994. Geologische Karte des Altkristallins östlich des Tauferer Tals (Südtirol). Erlanger geol. Abh. 124, 1–28.

Schwarz, S., Stöckhert, B., 1996. Pressure solution in siliciclastic HP-LT metamorphic rocks—constraints on the state of stress in deep levels of accretionary complexes. Tectonophysics 255, 203–209.

Shea, W.T., Kronenberg, A.K., 1992. Rheology and deformation mechanisms of an isotropic mica schist. Journal of Geophysical Research 97, 15,201–15,237.

Sibson, R.H., 1977. Fault rocks and fault mechanisms. Journal of the Geological Society, London 133, 191–213.

Simpson, C., 1985. Deformation of granitic rocks across the brittle–ductile transition. Journal of Structural Geology 7, 503–511.

Smith, D.L., Evans, B., 1984. Diffusional crack healing in quartz. Journal of Geophysical Research 89, 4125–4135.

Stöckhert, B., 1982. Deformation und retrograde Metamorphose im Altkristallin S′ des westlichen Tauernfensters (Südtirol). Unpublished Ph.D. thesis, University of Erlangen.

Stöckhert, B., 1984. K–Ar determinations on muscovites and phengites from deformed pegmatites, and the minimum age of the old Alpine deformation in the Austridic basement to the south of the western Tauern Window (Ahrn valley, southern Tyrol, eastern Alps). Neues Jahrbuch für Mineralogie, Abhandlungen 150, 103–120.

Tagami, T., Shimada, C., 1996. Natural long-term annealing of the zircon fission track system around a granitic pluton. Journal of Geophysical Research 101, 8245–8255.

Theye, T., Seidel, E., Vidal, O., 1992. Carpholite, sudoite, chloritoid in low-grade high-pressure metapelites from Crete and the Peloponnese, Greece. European Journal of Mineralogy 4, 487–507.

Tullis, J., 1983. Deformation of feldspars. Reviews in Mineralogy 2, 297–323.

Tullis, T.E., Tullis, J., 1986. Experimental rock deformation techniques. In: Hobbs, B.E., Heard, H.C. (Eds.), Mineral and Rock Deformation: Laboratory Studies. Geophysical Monograph 36, pp. 297–324.

Tullis, J., Dell'Angelo, L., Yund, R.A., 1990. Ductile shear zones from brittle precursors in feldspathic rocks: the role of dynamic recrystallization. In: Duba, A.G., Durham, W.B., Handin, J.W., Wang, H.F. (Eds.), The Brittle–Ductile Transition in Rocks. Geophysical Monograph 56, pp. 67–82.

Twiss, R.J., 1977. Theory and applicability of a recrystallized grain size paleopiezometry. Journal of Pure and Applied Geophysics 115, 227–244.

Twiss, R.J., 1986. Variable sensitivity piezometric equations for dislocation density and subgrain diameter and their relevance to olivine and quartz. In: Hobbs, B.E., Heard, H.C. (Eds.), Mineral and Rock Deformation: Laboratory Studies. Geophysical Monograph 36, pp. 247–261.

Voll, G., 1976. Recrystallization of quartz, biotite and feldspars from Erstfeld to the Leventina Nappe, Swiss Alps, and its geological significance. Schweizerische Mineralogische und Petrographische Mitteilungen 56, 641–647.

Wagner, G.A., Van den haute, P., 1992. Fission-Track Dating. Enke-Verlag, Stuttgart.

Wagner, G.A., Coyle, D.A., Duyster, J., Henjes-Kunst, F., Peterek, A., Schröder, B., Stöckhert, B., Wemmer, K., Zulauf, G., Ahrendt, H., Bischoff, R., Hejl, E., Jacobs, J., Menzel, D., Nand Lal, P., Van den haute, P., Vercoutere, C., Welzel, B., 1997. Post-Variscan thermal

and tectonic evolution of the KTB site and its surroundings. Journal of Geophysical Research 102, 18,221–18,232.

Weathers, M.S., Bird, J.M., Cooper, F.R., Kohlstedt, D.L., 1979. Differential stress determined from deformation-induced microstructures of the Moine thrust zone. Journal of Geophysical Research 84, 7495–7509.

White, S.H., Burrows, S.E., Carreras, J., Shaw, N.D., Humphreys, F.J., 1980. On mylonites in ductile shear zones. Journal of Structural Geology 2, 175–187.

Yamada, R., Tagami, T., Nishimura, S., Ito, H., 1996. Annealing kinetics of fission track in zircon: An experimental study. International Workshop on Fission-Track Dating, Gent, Abstr., 131.

Zoback, M.D., Harjes, H.-P., 1997. Injection-induced earthquakes and crustal stress at 9 km depth at the KTB deep drilling site, Germany. Journal of Geophysical Research 102, 18,477–18,491.